Thermal healing of realistic flaws in glass

Marco Zaccaria[1] and Mauro Overend[2]

[1]BE, MSc, Department of Engineering, University of Cambridge, UK, corresponding author, email mz287@cam.ac.uk

[2]BE&A, MSc, PhD, CEng MIStructE MICE, Senior Lecturer in Building Engineering Design, University of Cambridge, UK, email: mo318@cam.ac.uk

Abstract

For any given environmental conditions the tensile strength of glass is a function of the geometry of the critical flaw and the residual stresses in the vicinity of the flaw. The strength of heat treated glass is conventionally considered to be equal to the sum total of the residual stress and the extrinsic strength of annealed glass. Recent experiments suggest that there is an additional contribution to strength due to crack healing. In order to quantify it, uniaxial and equibiaxial strength tests on both as-received and carefully annealed glass specimens were performed for different edge geometries and edge finishes. The results show that strength recovery due to healing is significant and this strength gain appears to correlate with the quality of the edge finish. Possible explanations of this phenomenon are provided. Independently of healing effects, it was also found that the edge quality has a marginal effect on the mean strength, but has a significant positive effect at low fractile values often used in design applications.

Keywords: edge strength, surface strength, crack healing, residual stress.

Introduction

Over the past century glass has been used in increasing volumes in buildings. Its role has diversified: from simply supported panels for windows, to glass façades with ever increasing sizes of glass panels and smaller supported areas. The trend of using glass in a more structural manner extends to other applications such as staircases and roofs. Post-production processes such as tempering and lamination have brought about significant improvements in the performance of glass. However, the fundamental reasons for some of the strength and failure phenomena in glass are not fully understood.

Theoretically glass is a very strong material, with an intrinsic (i.e. flawless) tensile strength based on intermolecular forces as high as 32 GPa (Shelby 1997), but this is significantly reduced by stress concentrations at the tip of surface flaws. These flaws, also known as Griffith flaws, are unavoidable consequences of handling, transportation or in-service weathering and are generally found in large numbers on the surface of glass and can be classified as scratches or digs (Fig. 1). When the flaws are subjected to crack opening stresses (aka mode I loading), the stress concentration at the crack tip is described by the stress intensity factor K_I, which is a function of the shape and depth of the flaw. Irwin (1957) defined mode I loading as:

$$K_I = Y\sigma\sqrt{\pi a} \quad (1)$$

where,

Y is the geometry factor accounting for the shape of the crack,

σ is the tensile stress normal to the crack,

a is the crack depth.

It is particularly difficult to measure the flaw geometry and size prior to fracture. In fact, the flaw tip tends to be too small or between surfaces in close optical contact that is impossible to identify it from a top view with an optical microscope. Other instruments such as surface profilometers are equally unsuitable as they are unable to penetrate to the depth of the flaw tip. This difficulty is compounded further by the presence of median and lateral cracks (Fig. 2) that extend from the tip of the surface flaw. These cracks are formed when the glass is chipped or scratched, even when this is done by carefully controlled indentation or cutting (Schula and Schneider, 2013).

A common way of increasing extrinsic tensile strength of glass is tempering (thermal or chemical). These processes induce a residual stress state of compression in the surfaces regions of the glass and tension in the core of the glass. The compression on the surface enables the glass to resist tensile stresses at least as high as the residual stress, providing that there are no flaws deeper than the pre-compression layer. The processes of thermal and chemical tempering are not described here for brevity, but can be found in more specific literature (Haldimann et al. 2008, Zijlstra and Burggraaf 1968).

Commercially annealed glass is not entirely stress-free, in fact a small degree of residual stress, ranging from 4-11 MPa, has also been reported on as-received (commercially annealed) soda-lime-silica glass from float plants. This residual stress in commercially annealed glass is attributed to the cooling step in the annealing lehr of the float process which is not sufficiently slow to prevent residual stress from forming altogether (Zaccaria and Overend 2012). In this paper the term “annealed glass” is used to describe soda-lime-silica glass that is free of residual stress. The laboratory process performed to achieve this is described in subsequent parts of this paper.

Recently it was observed (Nielsen et al. 2010) that the extrinsic strength (f_{FT}) of fully tempered glass (FTG) is not simply the sum total of the extrinsic strength of annealed glass (f_{AN}) and the surface residual stress (σ_{RES}):

$$f_{FT} \neq f_{AN} - \sigma_{RES} \quad (2)$$

But an additional strength is also recorded, leading to:

$$f_{FT} = f_{AN} - \sigma_{RES} + f_{HEAL} \quad (3)$$

where f_{HEAL} is a strength gain due to crack healing.

A similar additional strength has been recorded (Zaccaria and Overend 2014) for chemically tempered glass (CTG) suggesting that equation (3) could be extended to all glasses that are subjected to a temperature profile of the type used in post-production processes. Equation (3) indicates that the extrinsic strength is governed by the critical flaw, residual stress and healing and is usually obtained from destructive tests, but the contribution from healing is not fully characterised.

Crack healing can be defined as a spontaneous process consisting of crack closure associated with a strength recovery. Griffith (1920) postulated that cracking could be a reversible process only in the case of very narrow cracks, i.e. when the two cracked surfaces correspond to one another and there is no debris between them.

Several researchers have studied the underlying causes of crack healing. The main parameters investigated are humidity and temperature profile. Healing was measured in terms of the energy required to re-open an artificial crack and in some studies was also observed visually.

Crack healing was investigated in humid and inert conditions, noticing that humidity prevents re-bonding by triggering chemical reactions at the flaw tip (Wiederhorn and Townsend 1970). Michalske and Fuller (1985) focused on the effect of controlled levels of humidity ranging from 0.01% to 100% and they also proposed a chemical model of

crack healing. The effect of temperature on crack healing was studied by Hrma et al. (1988), who investigated various temperature profiles and concluded that temperature favours healing, but that prolonged heat treatments lead to weakening. In a study by Inagaki et al. (1985) healing was observed visually on notched glass samples under cyclic loading and crack closure was ascribed to a mechanism similar to hysteresis. Crack closure was also visually observed by Girard et al. (2011), who took humidity and heat treatment into account and described healing as a step-by-step process involving relaxation of the stress immediately below the crack tip caused by indentation, crack blunting, followed by crack closure.

The existing body of research identifies the main factors that appear to affect crack healing in glass. All of the studies were performed by creating an artificial crack in glass and subsequently measuring the energy required to re-open it. These studies provide very useful information, but the phenomenon merits further investigation, in particular, to quantify:

1- The extent to which realistic (rather than indented) flaws are affected by crack healing. Realistic (Griffith) flaws would be expected to be more susceptible to healing, due to their size and optical contact, but this has yet to be ascertained;
2- The true strength gain resulting from thermal crack healing. In fact, any thermal treatment typically produces not only a residual stress (σ_{RES}), which enhances its performance, but also an additional strength due to healing (f_{HEAL});
3- The effect of thermal crack healing on a realistic flaw population rather than on a single flaw, and the strength increase at lower fractile values (rather than simply on the mean strength) as these values are important in real-world applications.

The aim of this paper is to quantify the strength gain of glass due to crack healing (f_{HEAL}) as a result of temperatures encountered during an annealing cycle. In doing so it

addresses the three principal gaps in knowledge listed above. This is done by carefully annealing as-received soda-lime-silica float glass. Annealing has the benefit of removing any remaining residual stress in the glass while providing a heating cycle below its transition temperature, thereby leaving the atomic structure unaffected. The annealed glass is subsequently tested to destruction and these results are compared to strength data obtained from as-received glass. To account for different realistic flaw populations, one type of untreated glass surface and three types of industry standard edge finish are tested on a coaxial double ring (CDR) and a 4-point bending (4PB) set-up, respectively. The strength contribution of residual stress (σ_{RES}) is determined by photoelastic measurements with a scattered light polariscope (SCALP) (Anton and Aben 2003).

Method

Standard soda-lime-silica glass (SLSG) has been used in this study. Its expected chemical composition and properties are shown in table 1 and table 2, respectively.

Four series were investigated (Table 3), each consisting of:

- 16 as-received float glass;
- 16 as-received float glass subsequently annealed in the laboratory.

The series were tested as follows:

- Series I coaxial double ring (CDR), size of the specimens 150 x 150 x 6mm;
- Series II, III, IV four point bending (4PB), size of the specimens 150 x 20 x 6 mm.

The three series tested in 4PB differ from one another in terms of edge finish: as cut, chamfered grinded, chamfered polished (Figure 3).

Surface pre-compression was measured with a calibrated scattered light polariscope (SCALP 5.0).

147 Specimen edges were investigated before and after annealing by means of an optical
148 microscope to identify any changes in flaw morphology.
149
150 *Coaxial double ring tests*
151 A CDR setup was used to test the surface strength of as-received and annealed glass
152 (Fig. 3). The glass specimens were tested using a universal testing machine with a 30 kN
153 load cell. The diameters of the loading and support rings were 51 mm and 126 mm,
154 respectively. A double hinged connection was placed between the cross-head and the
155 loading ring to ensure uniform contact between the loading ring and the glass. Before
156 testing, a UV-light detector was used to identify the tin side and all CDR specimens were
157 tested with the tin side in tension. A self-adhesive film was applied to the compression
158 side (air side) in order to hold the glass fragments together after fracture. The
159 specimens, jig sizes and the cross head speed comply with ASTM C 1499 (2003). The
160 crosshead speed of 0.02 mm/s was selected in order to fracture the specimens within 2
161 minutes, thereby limiting the effect of slow crack growth (Wiederhorn 1967 and Munz
162 and Fett 1999). The CDR setup induces an equibiaxial stress state on the surface of the
163 glass within the loading ring, therefore fracture is expected to originate at the largest
164 flaw within the loading ring, where the tensile stress is at its peak. Load at failure and
165 test duration were recorded.
166
167 *Four point bending*
168 A four point bending setup was used to test the strength of three different edge finishes
169 of as-received and annealed glass. The edge finish was as follows (Fig. 4):
170 - As-cut: the edge is sharp and might not be perfectly straight; density of flaws is
171 not controlled (DIN 1986);

- Grinded: the edge is chamfered and grinded; chips and flaws are allowed; the finish is opaque (DIN 1986);
- Polished edge: the edge is chamfered and polished; flaws and chips do not occur; slight polishing marks are allowed; the surface finish is shiny (DIN 1986).

All chamfers are 1.5 mm long at an angle of 45^{O}. The different edge finish affects the morphology and the density of the flaws, which will directly affect the stress at failure. However, the effect of the flaws cannot be quantified non-destructively, but can be determined by comparing the stress at failure.

The universal testing machine used is the same as for the CDR tests, fitted with a 4PB jig that loads the 150 mm long glass specimens at third points (i.e. 50mm sheer span and 50 mm load span). A double hinged connection between the crosshead and the loading arm allows the load to be applied uniformly. The sizes of the specimens and the jigs comply with ASTM C 1161 (2008). A crosshead speed of 0.02 mm/s was used in these tests, to induce fracture within 2 minutes.

The 4PB setup induces bending about the major axis of the specimens, thereby resulting in a uniaxial tensile stress state which is constant along the 50 mm load span length of the bottom edge (as-cut/grinded/polished). Fracture is therefore expected to originate at the largest flaw within the load span. A transparent self-adhesive tape was applied on both sides of the beam in order to retain glass fragments together after fracture.

Annealing and surface microscopy

Annealing was performed in the laboratory to remove the residual stress from the as-received glass. The annealing cycle was identical to that used by El-Sayed and Hand (2011) i.e. heating the glass at a rate of 2^{o}C/min up to 560^{o}C, holding for 2 hours and then cooling it at 2^{o}C/min to room temperature.

Edges of series II, III and IV were also examined with an optical microscope before and after the annealing process (Fig. 5). Flaws were recorded and measured. The investigation was carried out to establish whether the annealing process had caused any visible morphological changes in the flaws.

Photoelastic stress measurements

Residual stresses were measured for all the specimens with a SCALP. One reading per side per specimen was performed. For the series I the reading was made in the middle of the plate where failure was expected to originate. For the remaining series II, III, IV, although failure was expected to originate at the edges, it was not possible to measure the residual stress at this location due to restrictions of the device (Glasstress Ltd, Scattered Light Polariscope SCALP instruction manual ver 5.5, unpublished).

A measurement representative of the residual stress of the specimen was therefore made on the 20 mm side, parallel to the length of the specimen (Fig. 5). Typical SCALP measurements are shown in Fig. 7 and 8 for as-received and annealed specimens, respectively. The arithmetic mean of the residual stresses obtained for the respective series are shown in table 5. Edge working in the form of cutting, grinding and polishing is also expected to produce residual stresses in the vicinity of the edge, but it was not possible to measure this and these residual stresses are assumed to be relatively constant within each series thereby having a negligible effect on the comparisons made in this paper.

Results

Stress at failure was calculated using Kirchhoff-Love plate theory for CDR tests and Euler-Bernoulli beam theory for the 4PB tests.

For CDR tests, in the particular case of annular loading and support stress at failure equals (ASTM C 1499-2003 and Young et al. 2002):

$$\sigma_f = \frac{3L}{2\pi h^2}\left[(1-\nu)\frac{\emptyset_S^2-\emptyset_L^2}{2\emptyset^2} + (1+\nu)ln\frac{\emptyset_S}{\emptyset_L}\right] \quad (3)$$

where,

L is the load at failure in N,

h is the glass thickness in mm,

$\emptyset_S$ is the diameter of the reaction ring in mm,

$\emptyset_L$ is the diameter of the loading ring in mm,

ν is the Poisson ratio

$\emptyset$ is the diameter of a circle that expresses the characteristic size of the plate and for a squared plate can be expressed as follows:

$$\emptyset = \frac{l}{0.90961+0.12652\frac{h}{\emptyset_S}+0.00168\, ln\frac{l-\emptyset_S}{h}} \quad (4)$$

where l is the length of the side of the square glass specimen in mm.

For the 4PB tests, the reduction in second moment of area due to the chamfers was taken into account, as failing to do so would lead to an error of 11.6% in tensile stress. The relatively simple equations are not shown here for brevity.

In order to compare data independent of stress history, failure stresses were converted to a 60 s equivalent stress (Haldimann et al. 2008 and Overend and Zammit 2012). This represents the constant tensile stress to which the given specimen should be subjected in order to induce failure after 60 seconds. In the general case this can be expressed as follows:

$$\sigma_{t60} = \left[\frac{1}{t_0}\int_0^{t_f}\sigma^n(t)dt\right]^{1/n} \quad (5)$$

where,

σ_{t60} is the 60 s equivalent stress,

t_0 is the equivalent time period, (60s),

$\sigma(t)$ is the stress history,

t_f is the time at failure of the test,

n is the slow crack growth parameter, 16 for float soda-lime-silica glass (Haldimann et al. 2008).

For the case of constant stress rate used in this study, Eq. (5) can be re-written as follows:

$$\sigma_{t60} = \sigma_f \left[\frac{t_f}{t_{60}(n+1)}\right]^{1/n} \quad (6)$$

Mean 60 s equivalent failure stresses are shown in table 4.

Two-parameter Weibull statistical analysis was performed on the 60 s equivalent failure stresses. The method of moments (EN 12603-2002) was used to find the best fitting 2-parameter Weibull curve to the given test data. Table 6 shows: the resulting Weibull parameters θ and β, representing the scale parameter and the shape parameter, respectively; the Anderson-Darling goodness-of-fit statisticρ_{AD}; and the 0.001 and 0.5 fractile strengths, $f_{f;0.001}$ and $f_{f;0.5}$, respectively. The corresponding cumulative Weibull plots are shown in Figs. 9-12.

The mean strength increase due to healing, $\overline{f}_{\text{Heal}}$ for each series can be determined by re-arranging Eq. (3) and accounting for any residual stress that is present after the laboratory annealing (σ_{ResAN}), giving:

$$\overline{f}_{Heal} = \frac{1}{16}\sum_{i=1}^{16}\left[\left(f_{AN,t60} + \sigma_{ResAN}\right) - \left(f_{AR,t60} + \sigma_{ResAR}\right)\right]_i \quad (7)$$

where,

$f_{AN,t60}$ is the 60 s equivalent strength of the i-th annealed glass specimen,

σ_{ResAN} is the surface residual stress of the i-th annealed specimen,

$f_{AR,t60}$ is the 60 s equivalent strength of the i-th as-received glass specimen,

σ_{ResAR} is the surface residual stress of the i-th as-received specimen,

16 is the number of specimens for each batch.

The expressions in the first and second parenthesis of Eq. (7) are a measure of the extrinsic strengths of annealed and as-received glass, respectively. The difference between the extrinsic strengths of annealed and as-received glass is a measure of the strength gain due to healing. Equation (7) is in fact equivalent to:

$$f_{Heal,Px} = \left[\left(f_{AN,Px} + \bar{\sigma}_{ResAN}\right) - \left(f_{AR,Px} + \bar{\sigma}_{ResAR}\right)\right] \quad (8)$$

where, for each series,

$f_{Heal,Px}$ is the strength gain corresponding to the chosen fractile *Px*;

$f_{AN,Px}$ is the annealed glass strength corresponding to the chosen fractile *Px;*

$f_{AR,Px}$ is the as-received glass strength corresponding to the chosen fractile *Px.*

In this paper Eq. (8) has been used to calculate the extrinsic strength gain due to healing in each series at the 0.5 and 0.001 fractiles (table 7).

Comparison of flaws performed with an optical microscope before and after annealing did not reveal any morphological changes in the density of the flaw. Typical micrographs from this study are shown in fig. 6 a-d for as-cut and polished edge finish (series II, IV). It was difficult to ascertain any differences in the depth of the flaws perpendicular to the plane of view, but there was no apparent change to the length along the plane of view and other visible morphological features.

Discussion

Thermal healing

The strength gain due to crack healing can be assessed by comparing the extrinsic strength of annealed glass with the extrinsic strength of as-received glass for each test

series. By considering mean values and 0.5 fractile (best-fit) values in table 7 it is evident that strength gain occurs for all series. There are however significant differences in the lower fractile (0.001) values. More specifically, the as-cut and the grinded series show an extrinsic strength loss, whilst the CDR and the polished series exhibit a gain in extrinsic strength. This suggests that healing can have a significant influence on the low fractile values typically used in real-world applications, but that this phenomenon is sensitive to the edge or surface quality. A further illustration of this can be seen in the Weibull plots in figs. 9-12, which show that heat treatment was successful in reducing the scatter of failure stress values (i.e. the gradient of the best-fit line) for smaller flaws (CDR and polished series) whilst it increased the scatter for specimens with larger flaws (as-cut and grinded series). Furthermore, the best-fit lines of the polished series are almost parallel, indicating that the strength gain is fairly consistent for all flaw sizes present on the polished edges.

The sensitivity of healing to edge/surface quality is confirmed further by considering the 4PB series alone. Here the strength gain appears to be correlated with the quality of the edge finish. More precisely, not only does the edge quality correlate with higher strength (as expected), but the extrinsic strength gain from thermal healing is also more significant. This trend is confirmed by the 0.001 fractile although in this case the improvement is from a significant strength loss for the as-cut series (-28.8%) to a moderate strength loss (-4.1%) to a substantial strength gain (+35.0%).

In comparison, series I showed healing for all the fractiles, but the healing had a much larger beneficial effect on the lower fractile strength. This suggests that of all the flaw populations considered in this study, healing was most effective for the smaller flaws encountered on the glass surface (series I).

318 Microscopical investigation of the edges before and after annealing did not show any
319 change in flaw morphology (Fig. 6). However this does not rule out that a morphological
320 change occurs at a smaller scale or on areas which are impossible to investigate with an
321 optical microscope. A comparison of the flaw size and morphology before and after
322 annealing would help to explain the nature of the healing mechanism. Currently it is
323 possible to measure it only after failure (Fig. 13), but not before, thereby ruling out the
324 possibility to know the flaw size before annealing. However, a possible explanation of
325 the thermal healing mechanism can be drawn by merging the findings of this
326 experimental investigation with the existing literature. In fact, it is likely that in the
327 vicinity of the flaw tip a combination of applied stress, morphology of the flaw and
328 humidity affect the strength before and after heat treatment. Namely, in as-received
329 float glass (before heat treatment) (Fig. 14a):

330 - A residual stress profile with compression on the surface and tension in the core
331 exists. This is typical of as-received float glass;
332 - There is humidity at the flaw tip.
333 - The crack is formed and its geometry is characterised by a sharp tip;
334 - This is immediately followed by the formation of radial/median/lateral cracks
335 just below the flaw tip (Schula and Schneider 2013);
336 - Crack formation also causes local stresses at the flaw tip, similarly to those
337 generated during an indentation (Anunmana et al. 2009);

338 After heat treatment (annealing) (Fig. 14b):

339 - The residual stress profile is relaxed as confirmed by the photoelastic stress
340 measurements performed in this study;

- The crack retains its overall morphology as confirmed by the visual inspection (Fig. 6), but an optically invisible blunting at the crack tip may occur. This increases glass strength by reducing stress concentrations (Watson et al. 2013);
- And/or sub-critical cracks tend to close (re-bonding) as they match the definition of reversible cracks (Griffith 1920);
- Local stresses in the vicinity of the flaw tip undergo relaxation (Girard 2011);
- If the crack surfaces are in close optical contact humidity levels at the tip would not rise instantaneously, thereby, leading to an apparent gain in strength (Wiederhorn and Townsend 1970,Michalske and Fuller 1985), but on its own it cannot explain the increase in strength observed in this study.

Edge strength

Another important finding independent of thermal healing, is that the quality of surface/edges (i.e. flaw density and morphology) investigated in this study (which are typical of those found in real-world applications) has a relatively small influence on the mean and 0.5 fractile strengths, but has a very significant effect at the low fractile strengths commonly used in design applications. For example, polished edges in the as-received glass are on average 4.7 MPa (3.5%) stronger than as-cut edges (table 4), but the strength of polished edges at the 0.001 fractile value is 39.4 MPa (114.2%) higher than that of as-cut edges (table 6).This influence of edge finish at low fractile values is even more pronounced after thermal treatment (annealing). The reason for this sensitivity at low fractile values is that although the mean (and 0.5 fractile) values are only marginally affected by edge finish, the scatter of failure strengths (and implicitly the flaw sizes) are significantly reduced by grinding and more so by polishing. This is also evident in the magnitude of the shape parameter β in table 4 and manifests itself in

366 the increasing slope in the best-fit lines when comparing across fig. 10, fig. 11 and fig.
367 12.
368
369 **Conclusions**
370 This study showed that thermal healing of realistic flaws can induce a significant
371 strength gain in soda lime silica glass. This was quantified by testing as-received glass
372 specimens and glass specimens carefully annealed in the laboratory and comparing
373 their strength at failure. The effect on glass surface strength and on the edge strength of
374 three different edge finishes was considered. The results showed that the mean strength
375 increase for the glass surface, as-cut edges, and grinded edges was in the order of 1.9%
376 to 4.8%, but that this increase was 18.9% for polished edges. The effect of thermal
377 healing at low fractile values used in design applications (e.g. 0.001) was even more
378 pronounced for the polished edges with an increase as high as 35%, whilst as-cut and
379 grinded edges showed a decrease of 28.8% and 4.1%, respectively. The overall trend
380 was that a better quality edge finish resulted in a higher strength gain or healing.
381 This study also showed that for the low strength fractiles commonly used in design
382 applications, a good quality edge finish results in significantly higher edge strength.
383 Namely as-received polished edges proved to be 114.2% stronger than as-received as-
384 cut specimens. The same figure for average values is as low as 3.5% instead. The
385 benefits of a good quality edge finish at low fractile values are even more substantial
386 when glass undergoes thermal healing.
387 More work is required to better understand crack healing, in particular there is a need
388 to:
389 - Investigate different heating cycles. In fact cycles at a temperature higher than
390 the transition temperature may trigger increased morphological modifications

and changes at the atomic structure level. Also, thermal heating cycles typical of thermal tempering and chemical tempering could be of crucial importance for the application of these products;

- Investigate the morphological change of both natural flaws and artificially induced cracks, with the help of more powerful instruments, such as an atomic force microscope;
- Investigate crack healing for different surface flaws population (i.e. as-received glass vs naturally weathered glass) to determine whether healing has a similar effect on different surface flaw populations.

Acknowledgements

The contribution of Chris Cavanagh to part of the experimental testing, Trend Marine Ltd and EPSRCis gratefully acknowledged.

Notation list

The following symbols are used in this paper:

a = crack depth;

f_{AN} = extrinsic strength of annealed glass;

$f_{AN,Px}$ = annealed glass strength for a given fractileP_x;

$f_{AN,t60}$ = 60 s equivalent strength of the i-th annealed specimen;

$f_{AR,Px}$ = as-received glass strength for a given fractileP_x;

$f_{AR,t60}$ = 60 s equivalent strength of the i-th as-received specimen;

$f_{f;0.001}$ = 0.001 fractile strength;

$f_{f;0.5}$ = 0.5 fractile strength;

f_{FT} = extrinsic strength of fully tempered glass;

416 f_{HEAL} = strength gain due to healing;

417 $\overline{f}_{Heal}$ = average strength gain due to healing;

418 $f_{Heal,Px}$ = strength gain due to healing for a given fractileP_x;

419 h = glass specimen thickness;

420 K_I = stress intensity factor for mode I loading;

421 L = load at failure;

422 l = length of the side of the square glass specimen;

423 n = slow crack growth parameter;

424 t_0 = reference time period;

425 t_f = time to failure;

426 Y = flaw geometry factor;

427 β = surface strength shape parameter describing Weibull distribution;

428 θ = surface strength scale parameter describing Weibull distribution;

429 ν = Poisson's ration;

430 π = 3.14159265359;

431 ρ_{AD} = Anderson-Darling Weibull goodness of fit index;

432 σ= nominal tensile stress normal to the crack plane;

433 σ_f = stress at failure;

434 $\sigma^n(t)$ = stress history;

435 σ_{RES} = surface residual stress;

436 σ_{ResAN} = surface residual stress of the i-th annealed glass specimen;

437 $\bar{\sigma}_{ResAN}$ = average surface residual stress of annealed glass;

438 σ_{ResAR} = surface residual stress of the i-th as-received glass specimen;

439 $\bar{\sigma}_{ResAR}$ = average surface residual stress of as-received glass;

440 σ_{t60} = 60 s equivalent stress;

441 $\emptyset$ = diameter of a circle that express the characteristic size of the glass plate;

442 $\emptyset_L$ = diameter of the loading ring;

443 $\emptyset_S$ = diameter of the reaction ring.

444

445 **References**

446 Anton, J., Aben, H. (2003). "A compact scattered light polariscope for residual stress
447 measurement in glass plates." *Proc. Glass processing days,* Tampere, Finland.

448 Anunmana, C., Anusavice, K. J., Mecholsky, J.J., (2009). "Residual stress in glass:
449 indentation crack and fractography approaches." *Dent.Mater.,* 40(11), 1453-1458.

450 ASTM (2003)."Standard method for monotonic equibiaxial flexural strength of advanced
451 ceramics at ambient temperature."*C1499-03*, West Conshohocken, PA.

452 ASTM (2008)."Standard test method for flexural strength of advanced ceramics at
453 ambient temperature."*C1161-02c*, West Conshohocken, PA.

454 DIN (1986). "Glass in building; glass edges; concept, characteristics of edges types and
455 finishes." *1249-11:1986-09*, Berlin, Germany.

456 EN (2002). "Glass in building. Procedures for goodness of fit and confidence intervals
457 for Weibull distributed glass strength data." *12603:2002,* European committee for
458 standardization, Brussels, Belgium.

459 EN (2004). "Glass in building – Basic soda lime silicate glass products – Part 1:
460 Definitions and general physical and mechanical properties". 572-1:2004, European
461 committee for standardization, Brussels, Belgium.

462 El-Sayed, T., Hand, R. J. (2011). "Modelling the strengthening of glass using epoxy based
463 coatings." J. Eur. Cer. Soc., 31, 2783-2791.

464 Girard, R., Faivre, A., Despetis, F. (2011)."Influence of water on crack self-healing in
465 soda-lime silicate glass." *J. Am.Cer. Soc.*, 94, 2402-2407.

Griffith, A. A. (1920). “The phenomena of rupture and flow in solids.” *Phil.Trans. R. Soc., Series A,* 221, 163-198.

Haldimann, M., Luible, M., Overend, M. (2008).*Structural use of glass*.Struct. Eng.Doc. no. 10, International Association of Bridge and Structural Engineers.

Hrma, P., Han, W. T., Cooper, A. R. (1988).“Thermal healing of cracks in glass.”*J. non-cryst.solids,* 102, 88-94.

Inagaki, M., Urashima, K., Toyomasu, S., Goto, Y., Sakai, M. (1985). “Work of fracture and crack healing in glass.” *J. Am.Cer. Soc.,* 68, 704-706.

Irwin, G. (1957). “Analysis of stresses and strains near the end of a crack transversing a plate.”*J. Appl. Mech.,* 24, 361-364.

Michalske, T. A., Fuller, E. R. (1985). “Closure and repropagation of healed cracks in silicate glass.”*J. Am.Cer. Soc.,* 68(11), 586-590.

Munz, D., Fett, T. (1999).*Ceramics: mechanical properties, failure behaviour, materials selection.*Springer, Berlin and Heidelberg, Germany.

Nielsen, J. H., Olesen, J. F., Stang, H., (2010). “Characterization of the residual stress state in commercially fully toughened glass”. J. Mat. Civ. Eng., 22(2), 179-185.

Nielsen, J. H., Olesen, J. F., Poulsen, P. N., Stang, H. (2010). “Finite element implementation of a glass tempering model in three dimensions.”*Comp. and Struct.,* 88, 963-972.

Overend, M., Zammit, K. (2012). “A computer algorithm for determining the tensile strength of float glass” *Eng. Struct.,* 45, 68-77.

Shelby, J. E., (1997). *Introduction to glass science and technology.* Roy. Soc. Chem. Cambridge, UK.

Schula, S., Schneider J. (2013).“Characterization of the scratch visibility of annealed and tempered soda-lime-silicate glass.”*Proc,. COST Action TU0905, Mid-term Conference on Structural Glass,* Porec, Croatia.

Sullivan, J. D., Lauzon, P. H. (1986). “Experimental probability estimators for Weibull plots.”*J.Mat. Sc.,* 5, 1245-1247.

Varshneya, A. K. (2012). *Fundamentals of Inorganic Glasses,* The society of Glass Technology, Sheffield, UK.

Watson, J., Nielsen, J. H., Overend, M. (2013). “A critical flaw size approach for predicting the strength of bolted glass connections”.*Eng.Struct.,*57, 87-99.

Wiederhorn, S. M. (1967). “Influence of water vapour on crack propagation in soda-lime glass”. *J. Am.Cer. Soc.,* 50, 407-414.

Wiederhorn, S. M., Townsend, P. R. (1970). “Crack healing in glass.” *J. Am.Cer. Soc.,* 68, 486-489.

Young, W., Budynas, R., Sadegh, A. (2002).*Roark’s formulas for stress and strain, 7thed,* McGraw-Hill, New York, NY.

Zaccaria, M., Overend, M. (2012). “Validation of a simple relationship between the fracture pattern and the fracture stress of glass.”*Proc., Engineered Transparency,* Dusseldorf, Germany.

Zaccaria, M., Overend, M. (2014). “The mechanical performance of bi-treated glass.”*Proc.,Challenging Glass 4 & COST Action TU0905 Final Conference,* Lausanne, Switzerland.

Zijlstra, A. L., Burggraaf, A. J. (1968). “Fracture phenomena and strength properties of chemically and physically strengthened glass.” *J. Non-Cryst. Solids,* 1, 49-68.

List of tables

Figure captions

539 **Fig. 14.** Schematic explanation of crack healing: (a) flaw, as-received float glass, (b) in-
540 lab annealed glass.
541

Tables

Table 1. SLSG composition (% mass) according to EN (2004).

SiO_2	CaO	Na_2O	MgO	Al_2O_3	Others
69-74%	5-14%	10-16%	0-6%	0-3%	0-5%

546 **Table 2.** Relevant SLSG properties.

Property	**Symbol**	**Value**	**Source**
Density (kg/m^3)	ρ	2500	Haldimann et al. (2008)
Young's modulus (MPa)	E	70000	Haldimann et al. (2008)
Poisson ratio (-)	ν	0.23	Haldimann et al. (2008)
Stress intensity factor (MPa m$^{1/2}$)	K_{IC}	0.75	Overend and Zammit (2012)
Slow crack growth parameter	n	16	Overend and Zammit (2012)
Coefficient of thermal expansion (10^{-6}K^{-1})	α_T	9	Haldimann et al. (2008)
Glass transition temperature (^{o}C)	T_g	575	Shelby (1997)
Annealing point (^{o}C)	T_a	550	Shelby (1997)
Photoelastic constant (TPa)	C	3.01	Nielsen (2010)

547

548

549 **Table 3.** Summary of test specimens.

Series	Dimensions (mm)	Edge Finish	Test	# of specimens
I	150x150x6	N/A	CDR	16 as-received 16 annealed
II	150x20x6	As-cut	4PB	16 as-received 16 annealed
III	150x20x6	Grinded	4PB	16 as-received 16 annealed
IV	150x20x6	Polished	4PB	16 as-received 16 annealed

550

551

552 **Table 4.** Test data and 60 s equivalent failure stresses.

Series	Failure stress (MPa)		60 s equivalent stress (MPa)		Standard Deviation (MPa)	
	As-received	Annealed	As-received	Annealed	As-received	Annealed
I	179.3	181.0	147.3	148.9	74	51
II	173.1	172.6	134.5	135.2	28	38
III	170.2	175.0	135.0	139.4	21	23
IV	181.3	211.9	139.2	163.6	18	16

553

554

555 **Table 5.** Measured residual stresses.

Series	Mean Residual stresses (MPa)		Standard Deviation (MPa)	
	As-received	Annealed	As-received	Annealed
I	-4.6	-2.2	0.37	0.71
II	-4.2	-2.4	0.52	0.67
III	-4.4	-2.5	0.53	0.59
IV	-3.5	-2.2	0.61	0.56

556

557

558 **Table 6.** Weibull analysis of 60 s equivalent failure stresses.

	Series	Weibull Parameters		Goodness-of-fit	Fractile strengths	Fractile strengths
		θ	β	ρ_{AD}	$f_{f;0.5}$	$f_{f;0.001}$
I	As-received	175.6	2.02	0.071	146.4	5.7
	Annealed	167.0	3.27	0.11	149.7	20.3
II	As-received	148.9	4.72	0.11	137.8	34.5
	Annealed	*151.8*	*3.75*	*0.01*	*137.7*	*24.1*
III	As-received	145.0	6.80	0.32	137.5	52.5
	Annealed	151.3	6.08	0.29	142.5	48.6
IV	As-received	146.1	10.13	0.42	140.9	73.8
	Annealed	170.6	12.25	0.55	165.6	97.1

559 Note: values in italics indicate a poor Weibull fit.

560

561 **Table 7.** Summary of extrinsic strengths and strength gains.

Series	Extrinsic strength of Annealed glass (MPa) $f_{AN,Px} + \overline{\sigma}_{ResAN}$			Extrinsic strength of As-received glass (MPa) $f_{AR,Px} + \overline{\sigma}_{ResAR}$			Extrinsic Strength gain (MPa) f_{Heal}		
	Mean	**0.5**	**0.001**	***Mean***	**0.5**	**0.001**	***Mean***	**0.5**	**0.001**
I	146.7	147.5	18.1	142.7	141.8	1.1	4.0 (2.8%)	5.7 (4.0%)	17.0 (offlimits)
II	132.8	135.3	21.7	130.3	133.6	30.5	2.5 (1.9%)	1.7 (1.3%)	-8.8 (-28.8%)
III	136.9	140.0	46.1	130.6	133.1	48.1	6.3 (4.8%)	6.9 (5.2%)	-2.0 (-4.1%)
IV	161.4	163.4	94.9	135.7	137.4	70.3	25.7 (18.9%)	26 (18.9%)	24.6 (35.0%)

562

Click here to download Figure: Figure 1.tif

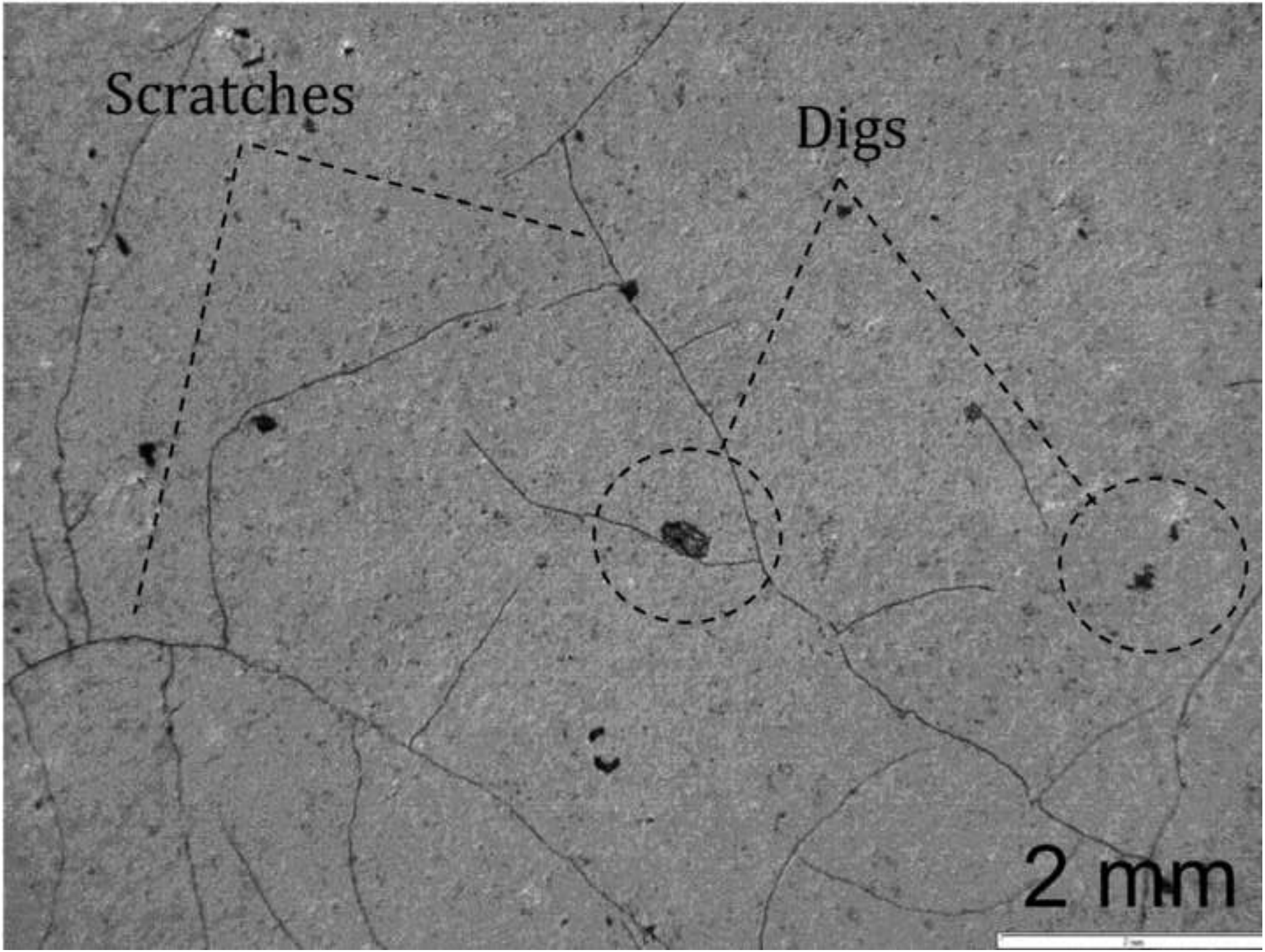

Click here to download Figure: Figure 2.tif

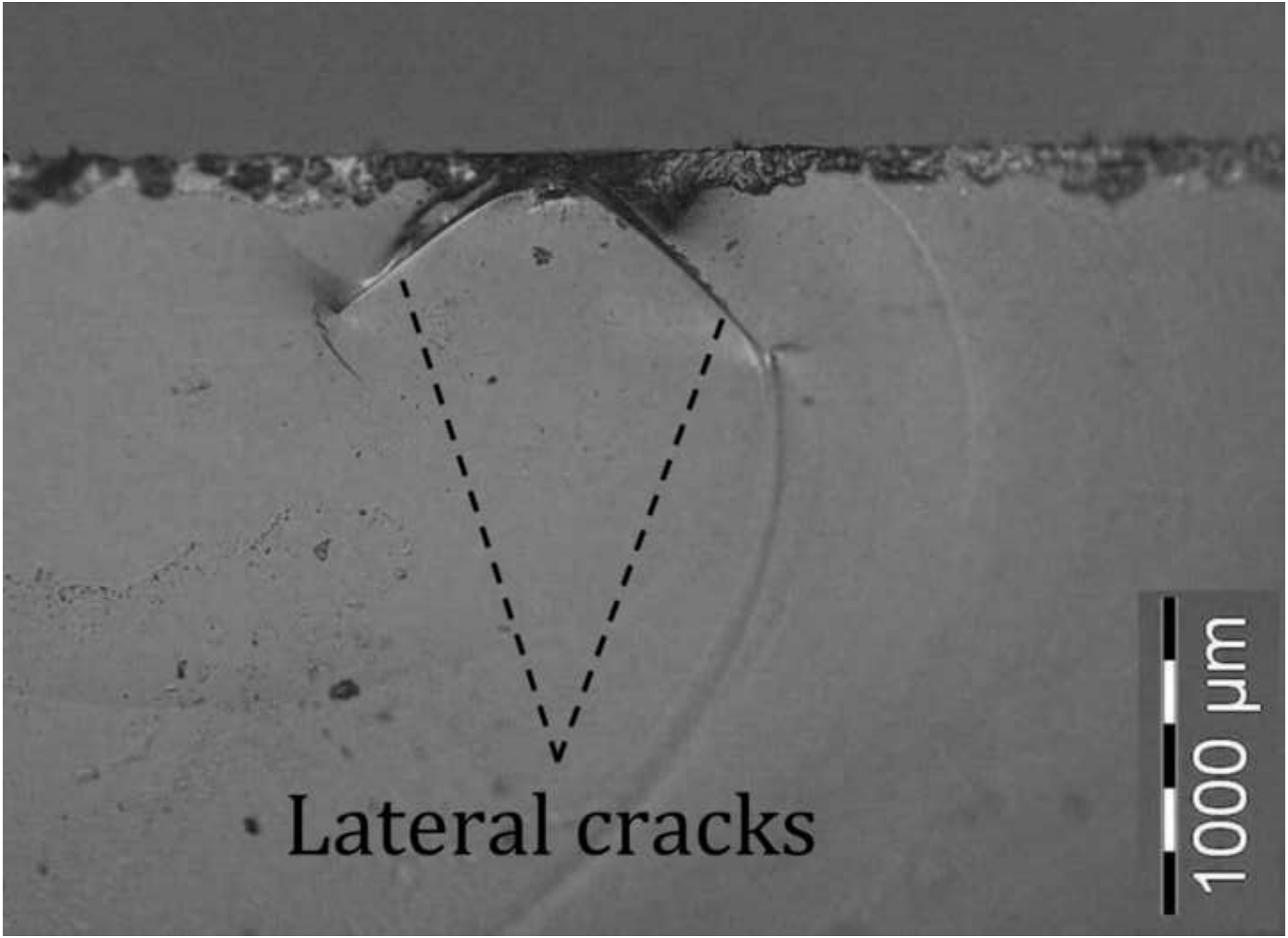

Click here to download Figure: Figure 3.tif

Click here to download Figure: Figure 4.tif

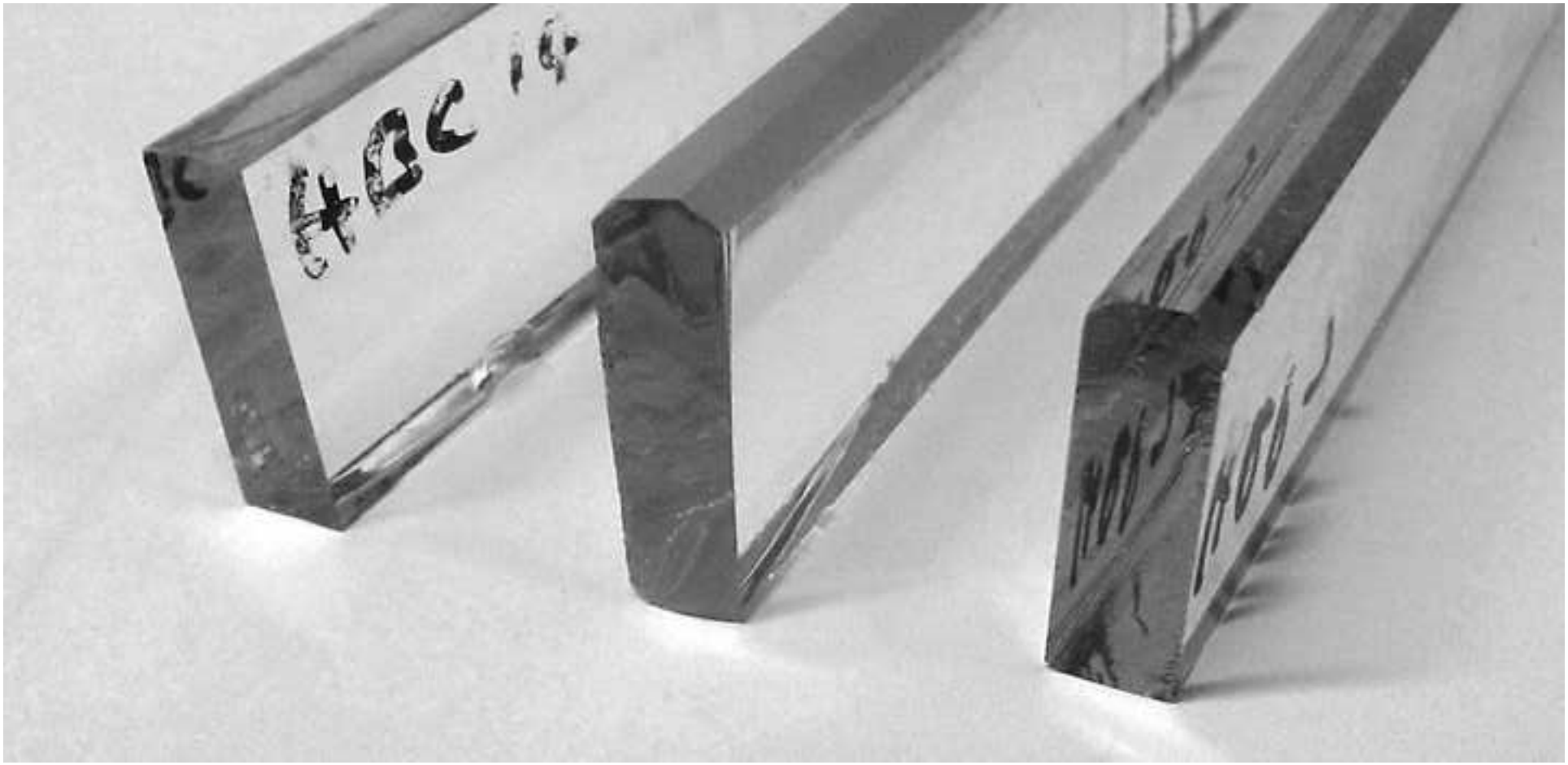

Click here to download Figure: Figure 5.jpg

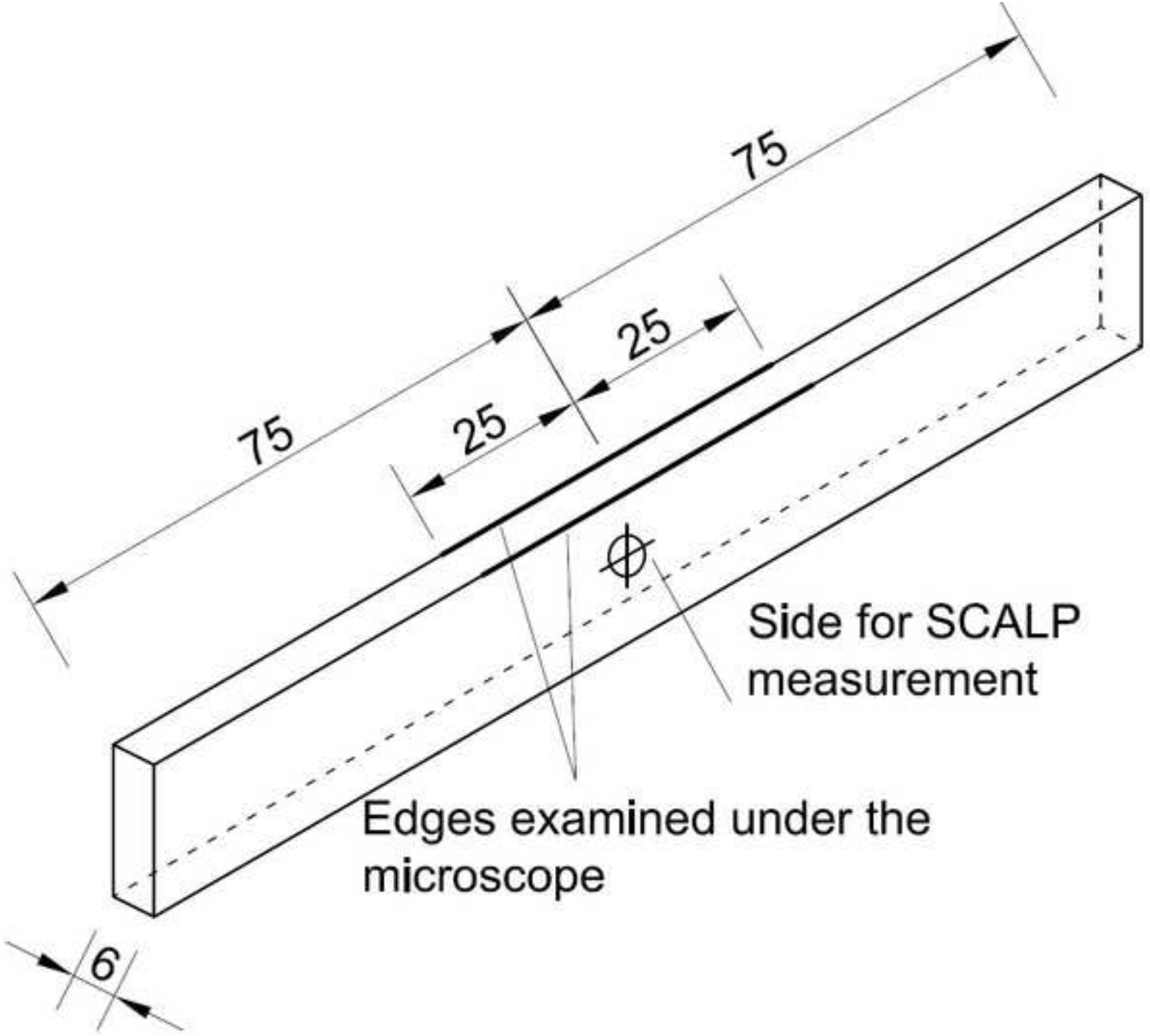

Click here to download Figure: Figure 6a.tif

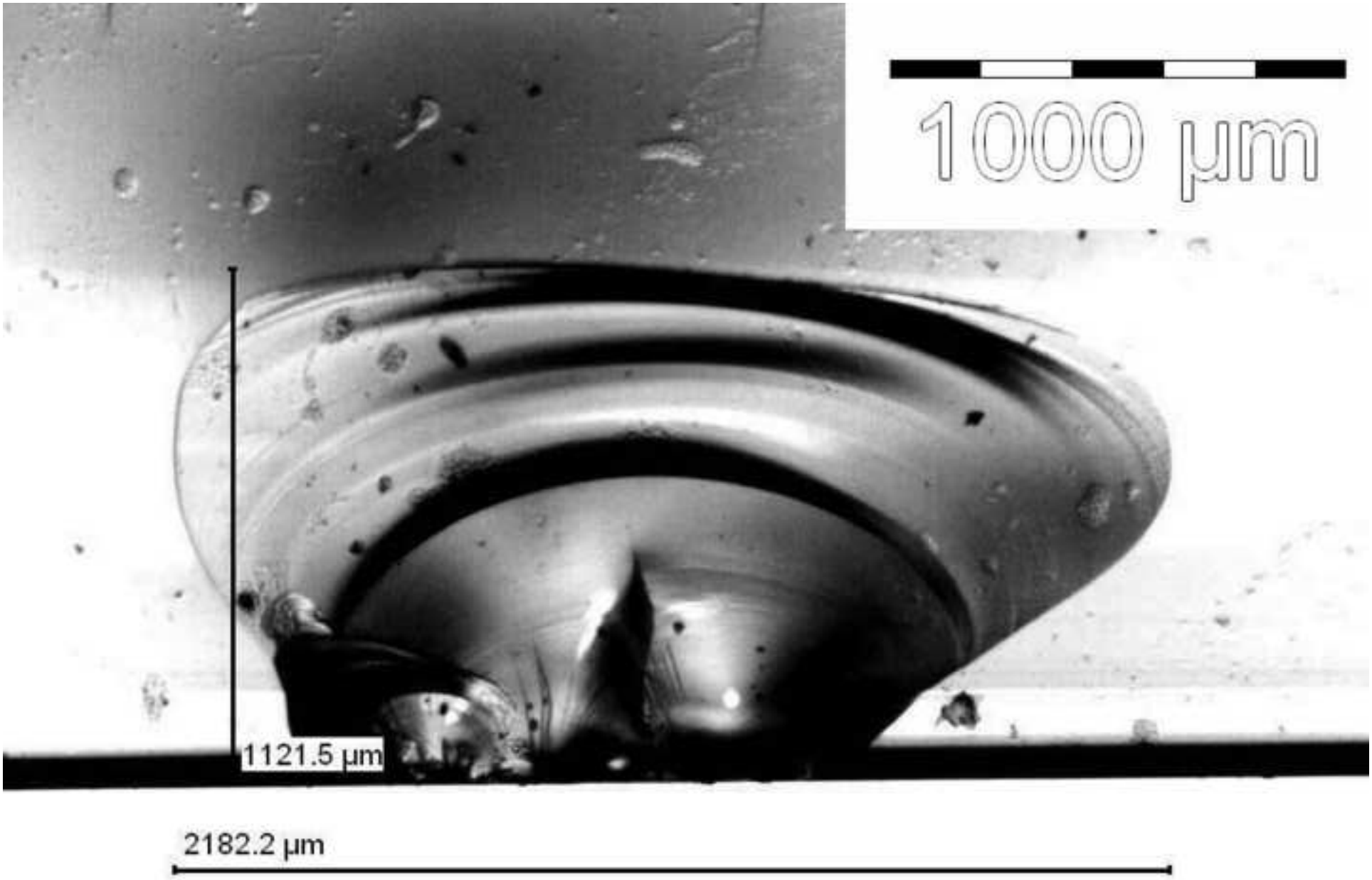

Click here to download Figure: Figure 6b.tif

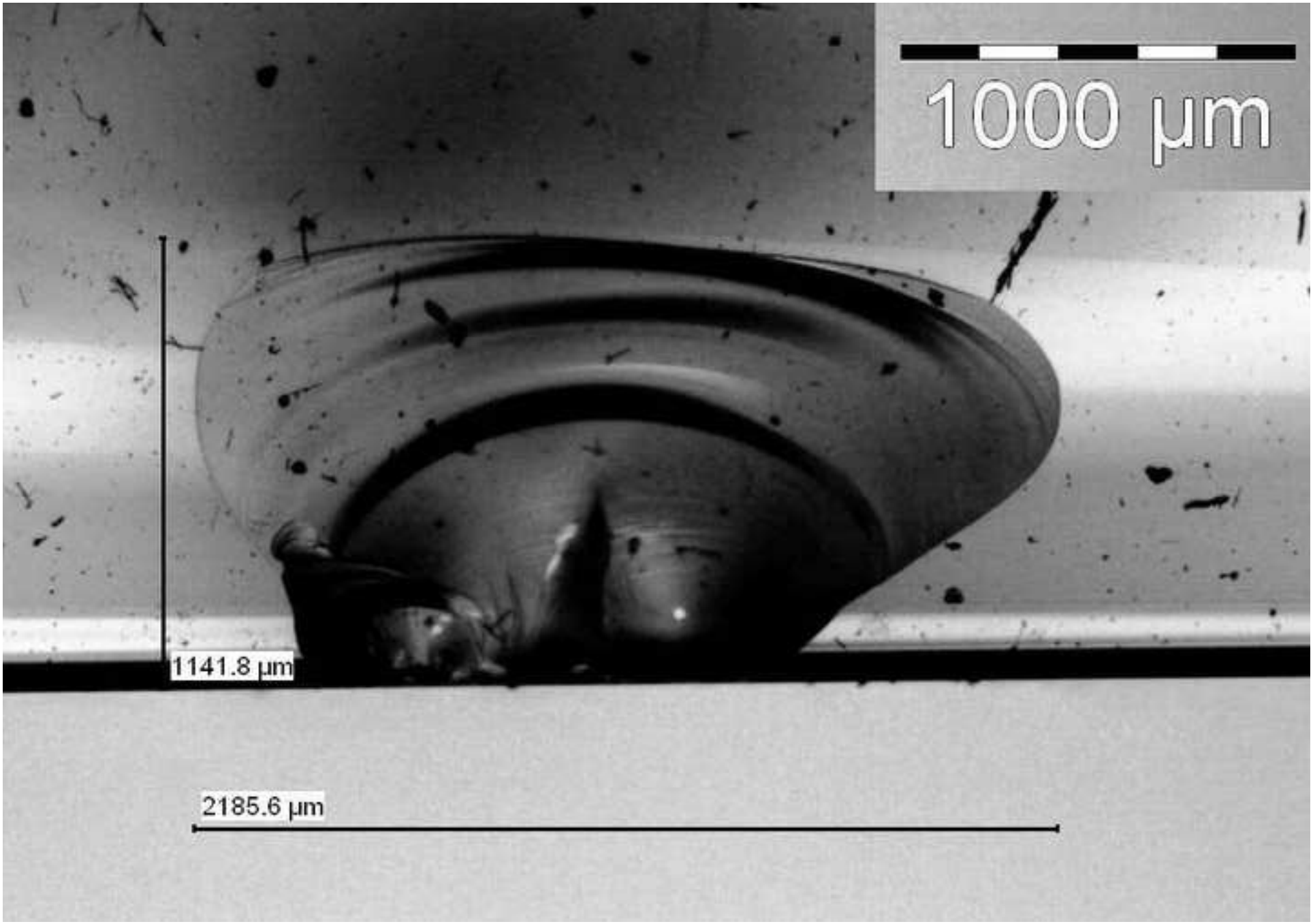

Click here to download Figure: Figure 6c.tif

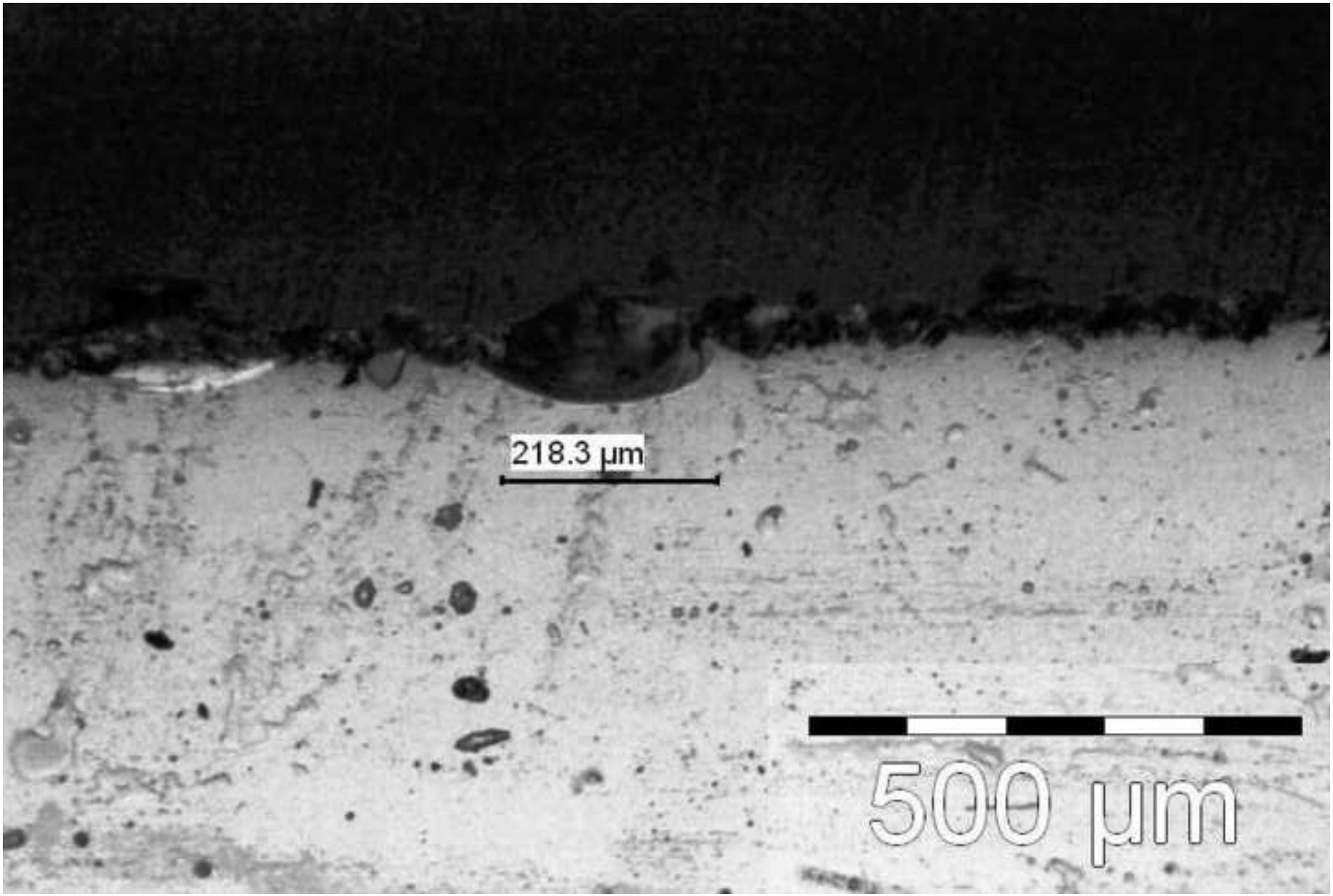

Click here to download Figure: Figure 6d.tif

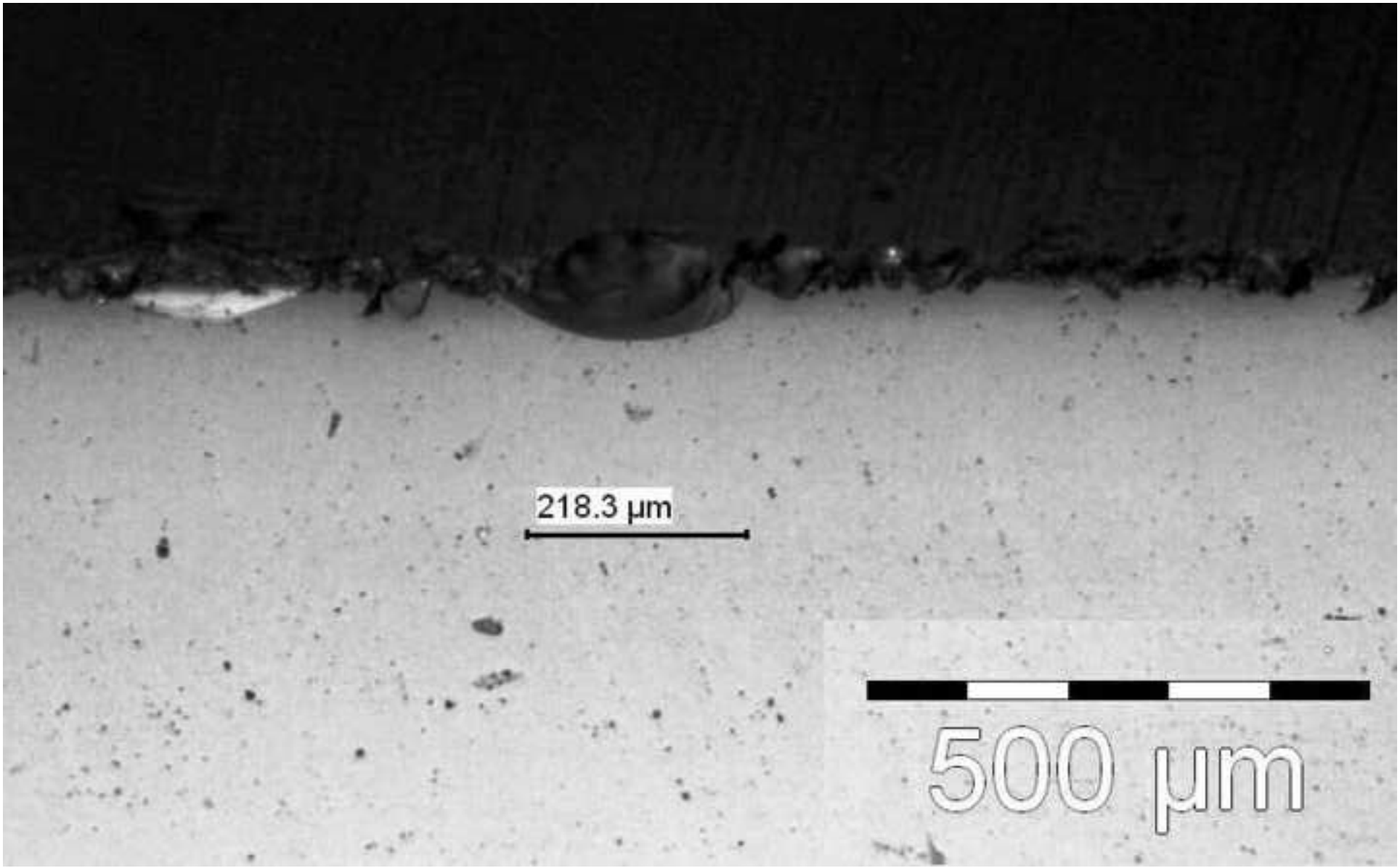

Click here to download Figure: Figure 7.tif

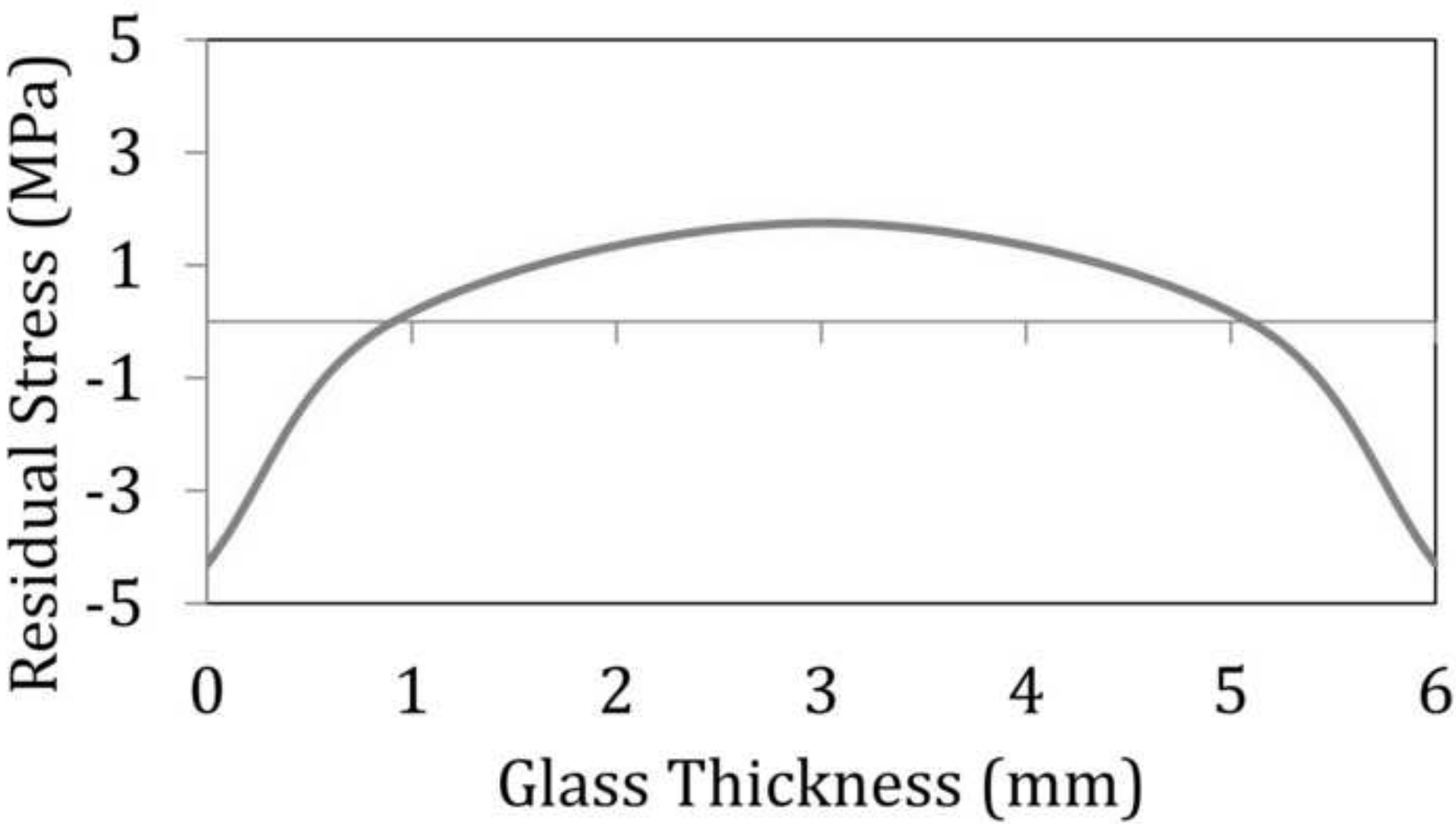

Click here to download Figure: Figure 8.tif

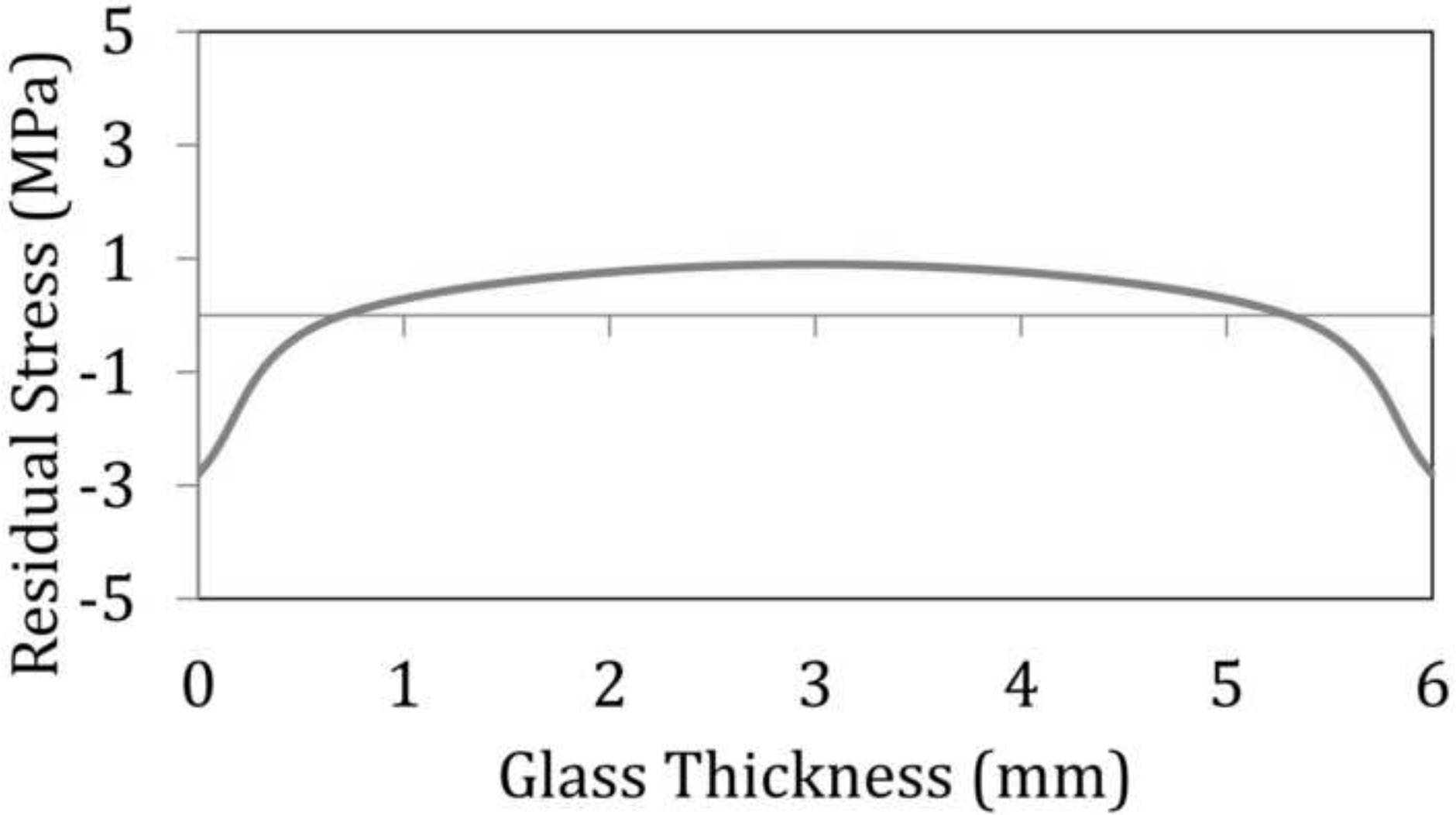

Click here to download Figure: Figure 9.tif

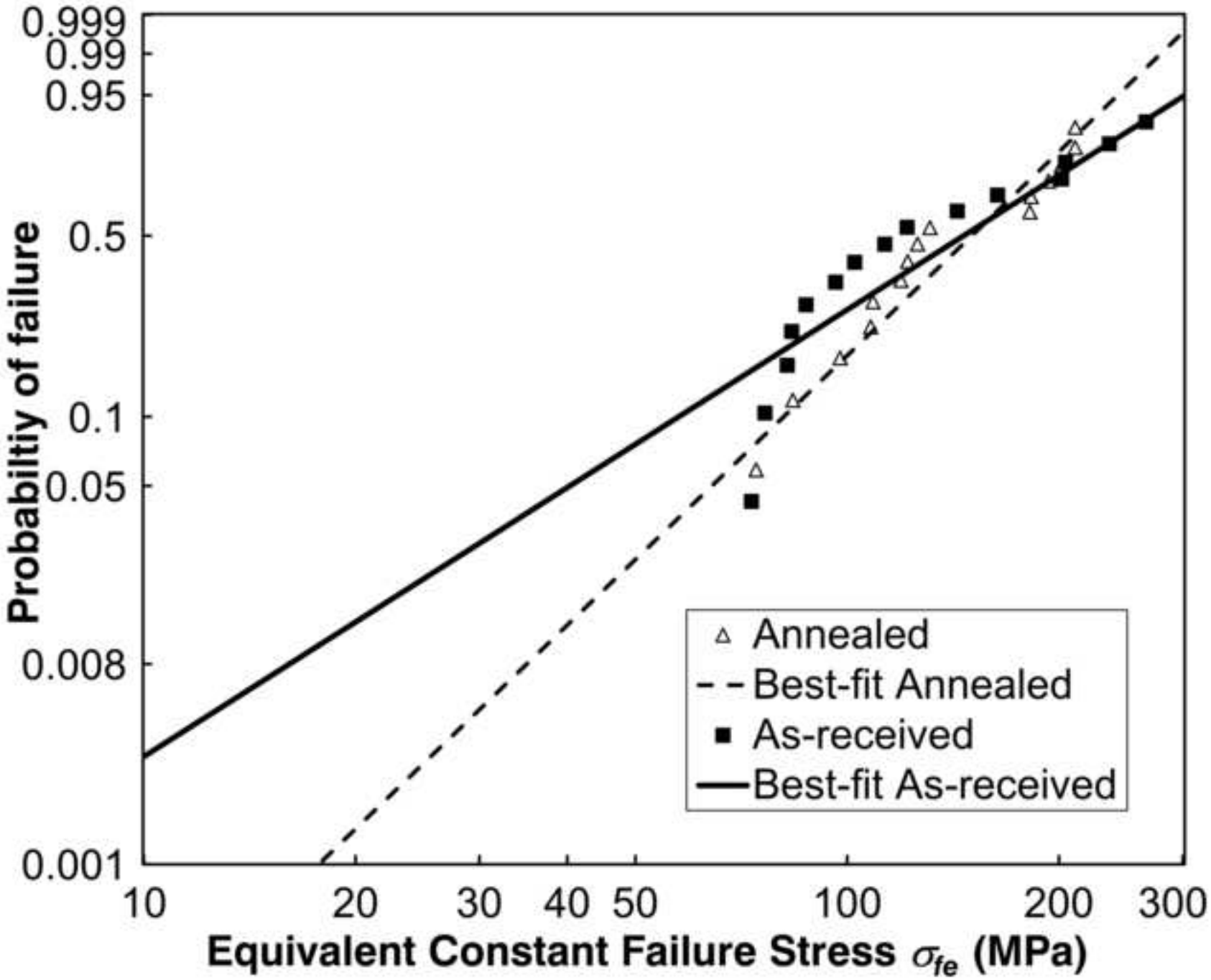

Click here to download Figure: Figure 10.tif

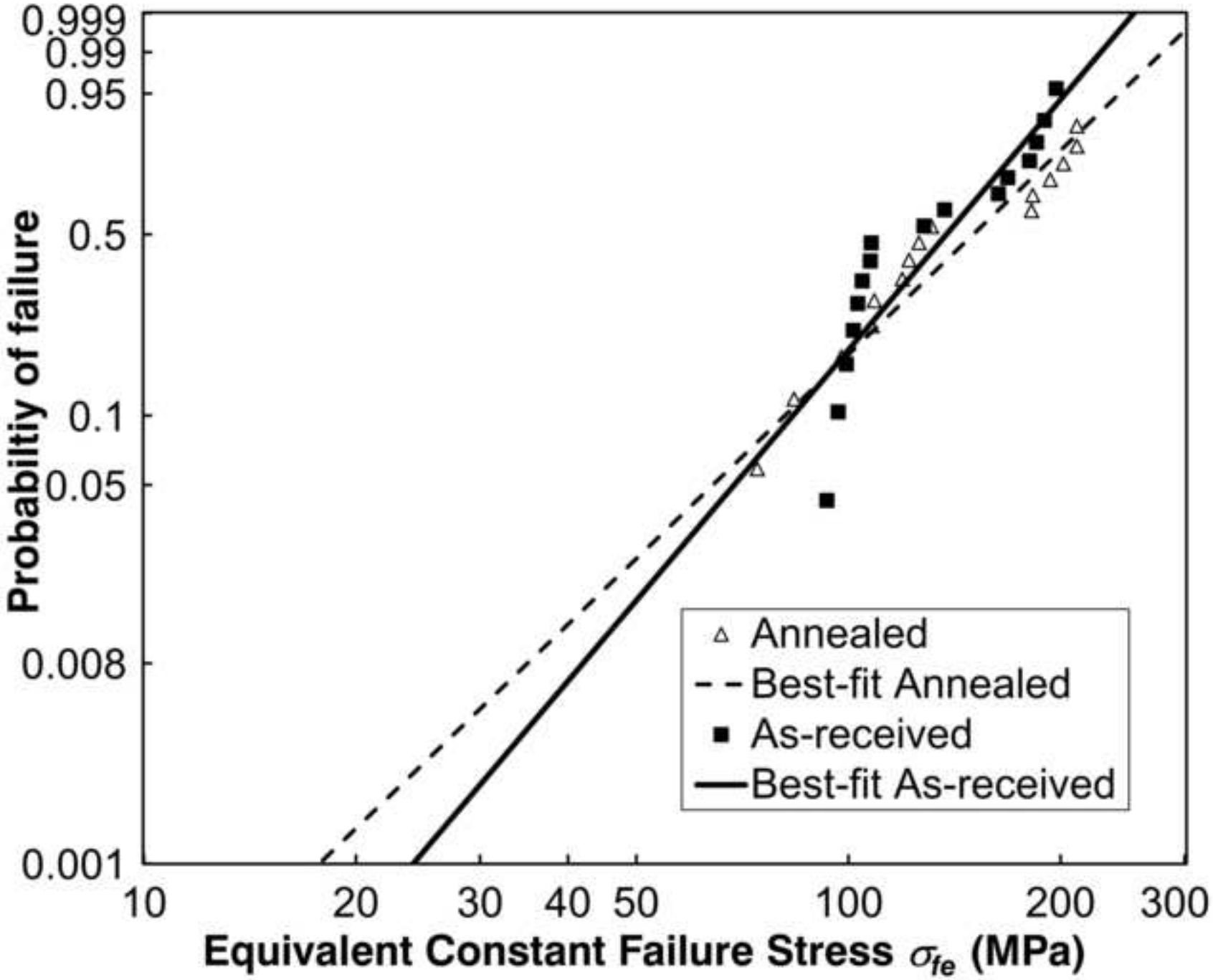

Click here to download Figure: Figure 11.tif

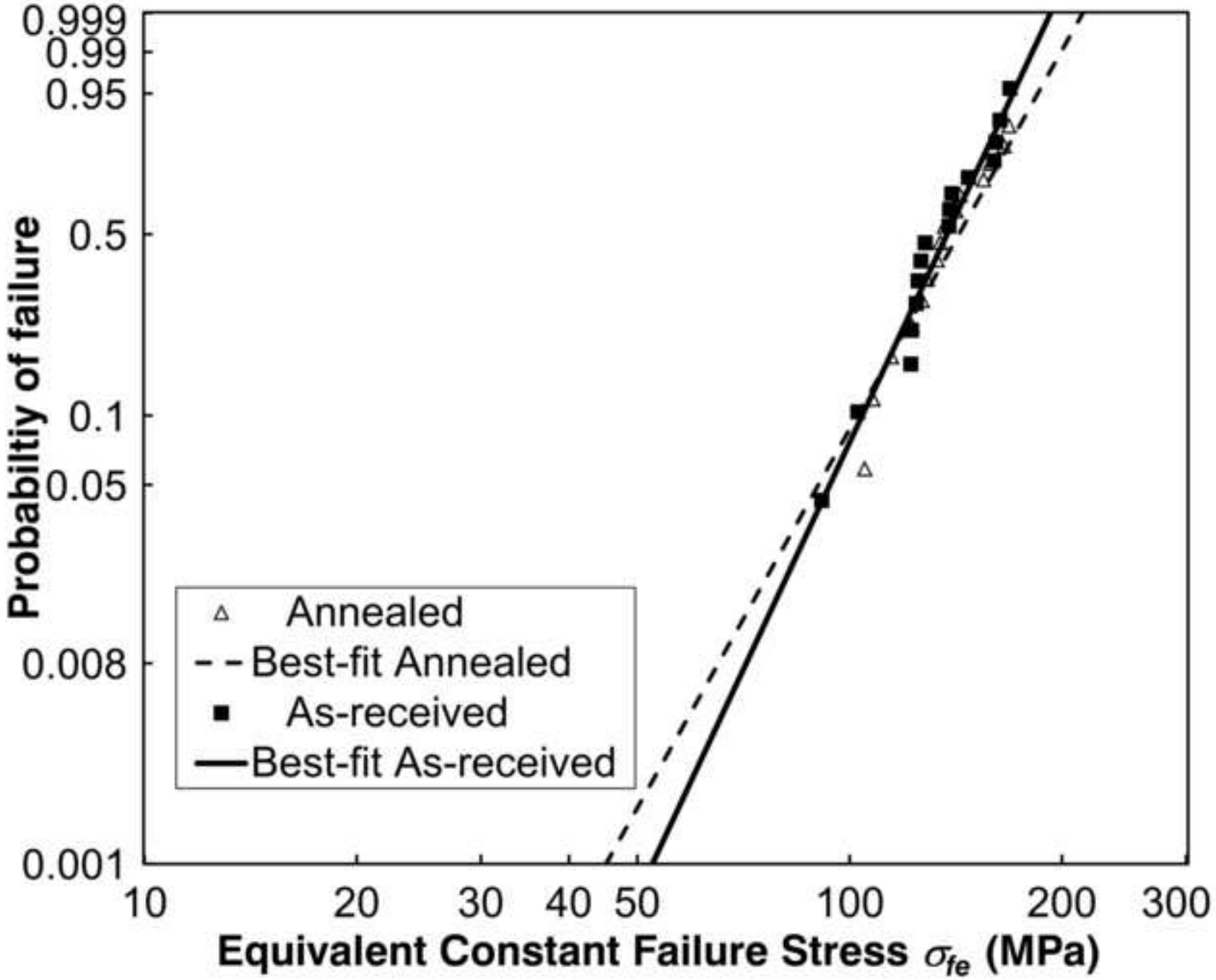

Click here to download Figure: Figure 12.tif

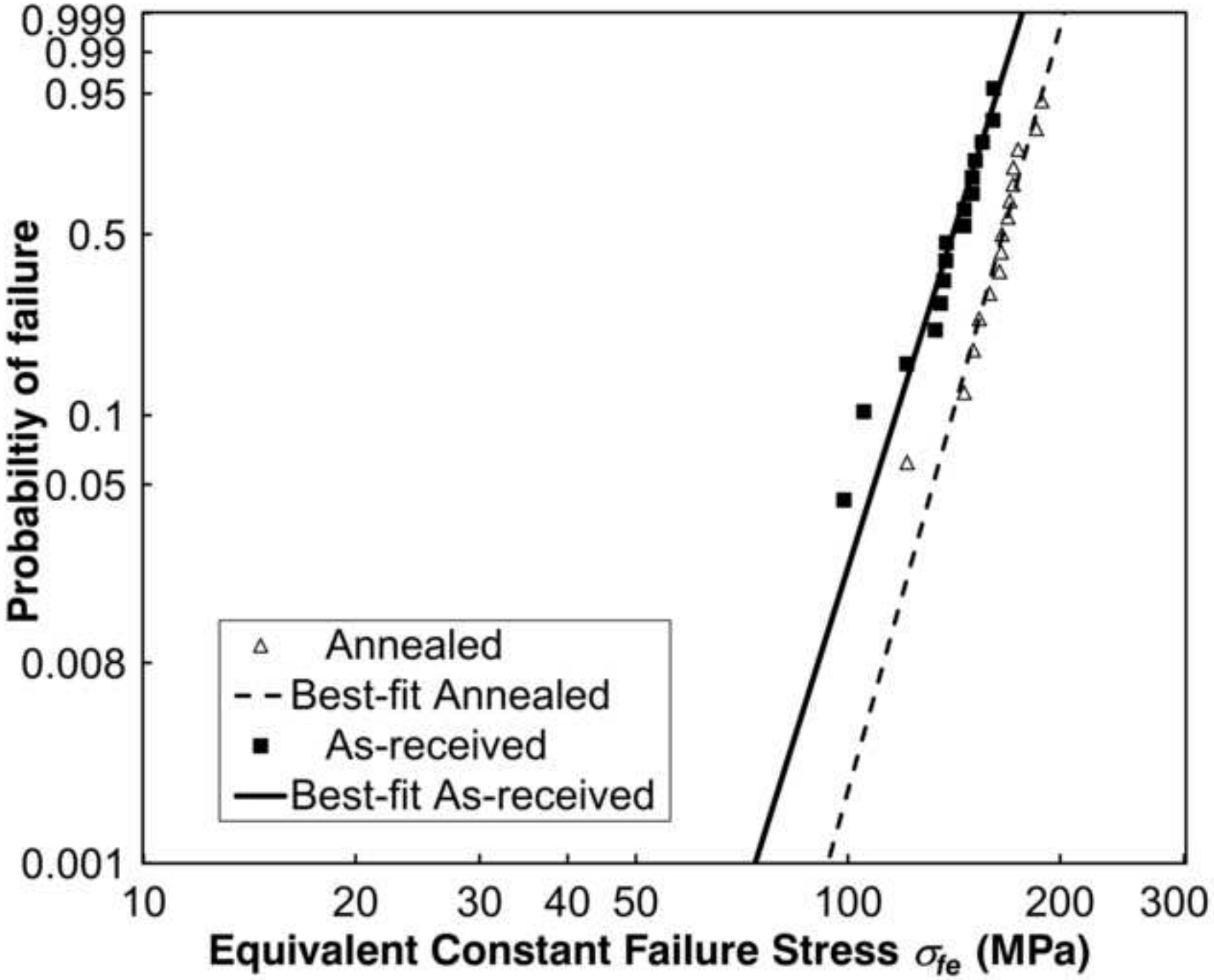

Click here to download Figure: Figure 13.tif